Oluwaseun Adedokun*, Omonike Mary Adedokun,
Ismaila Taiwo Bello*, Adegbenro Sunday Ajani, Peverga Rex Jubu,
Mojoyinla Kofoworola Awodele, Mokhotjwa Simon Dhlamini,
Ashok Kumar Kaliamurthy and Mashooq Ahmad Bhat

Sol–gel synthesized lithium–cobalt co-doped titanium (IV) oxide nanocomposite as an efficient photocatalyst for environmental remediation

https://doi.org/10.1515/zpch-2024-0835
Received April 5, 2024; accepted June 25, 2024; published online July 8, 2024

Abstract: In this study, lithium cobalt co-doped titanium oxide (Li:Co-TiO_2) was reported via the sol–gel method in a one-pot synthesis approach and their potential applications were evaluated for the photodegradation of organic dye as photocatalysts. The structural and optical properties of the photocatalysts were respectively elucidated using X-ray diffraction (XRD), Fourier transform infrared

***Corresponding authors: Oluwaseun Adedokun**, Department of Pure and Applied Physics, Ladoke Akintola University of Technology, P.M.B 4000, Ogbomoso, Nigeria; and Nanotechnology Research Group (NANO+), Ladoke Akintola University of Technology, Ogbomoso, Nigeria, E-mail: oadedokun@lautech.edu.ng. https://orcid.org/0000-0002-7947-8415 (O. Adedokun); and
Ismaila Taiwo Bello, Department of Physics, College of Science, Engineering and Technology, University of South Africa, Johannesburg 1710, South Africa, E-mail: belloit@unisa.ac.za. https://orcid.org/0000-0002-1109-9259 (I.T. Bello)
Omonike Mary Adedokun, Department of Pure and Applied Physics, Ladoke Akintola University of Technology, P.M.B 4000, Ogbomoso, Nigeria. https://orcid.org/0009-0001-0631-206X
Adegbenro Sunday Ajani, Department of Physics and Material Science, Faculty of Pure and Applied Sciences, Kwara State University, Malete, P.M.B 1530, Ilorin, Kwara State, Nigeria. https://orcid.org/0000-0003-1104-3500
Peverga Rex Jubu, Department of Physics, Joseph Sarwuan Tarkaa University Makurdi (JOSTUM), P.M.B. 2373, Makurdi, Benue State, Nigeria. https://orcid.org/0000-0002-5249-1273
Mojoyinla Kofoworola Awodele, Department of Pure and Applied Physics, Ladoke Akintola University of Technology, P.M.B 4000, Ogbomoso, Nigeria; and Nanotechnology Research Group (NANO+), Ladoke Akintola University of Technology, Ogbomoso, Nigeria. https://orcid.org/0000-0002-6719-8328
Mokhotjwa Simon Dhlamini, Department of Physics, College of Science, Engineering and Technology, University of South Africa, Johannesburg 1710, South Africa. https://orcid.org/0000-0002-4001-6408
Ashok Kumar Kaliamurthy, Department of Energy and Materials Engineering, Dongguk University, Seoul 04620, Republic of Korea. https://orcid.org/0000-0001-7851-0404
Mashooq Ahmad Bhat, Department of Pharmaceutical Chemistry, College of Pharmacy, King Saud University, P.O Box 2457, Riyadh 11451, Saudi Arabia. https://orcid.org/0000-0001-8426-4692

spectroscopy (FTIR), and diffuse reflectance spectroscopy (DRS). The morphological and elemental composition of the Li:Co-TiO_2 was established by high-resolution field-emission scanning electron microscopy (FESEM) coupled with EDX, which confirmed a successful preparation of the photocatalysts. The modification of TiO_2 with Li:Co changes the optical properties of the pristine TiO_2 with a reduction in the bandgap (3.26–2.8 eV) of the resultant photocatalysts. The photocatalytic activity of Li:Co-TiO_2 composites was examined for their efficacy through the degradation of Methylene Blue (MB) dye. The photodegradation revealed an improved performance of Li:Co-TiO_2 in the degradation of MB compared to pristine TiO_2. The total amount of the degraded MB dye within the total time interval of the irradiation was recorded to be 72 % and 87 % for TiO_2 and Li:Co co-doped TiO_2 respectively. The enhanced results obtained from the photocatalytic activity of Li:Co-TiO_2 to degrade MB, suggest that the composite is a potential candidate for environmental remediation and photocatalysis applications.

Keywords: Li:Co-TiO_2 composites; photocatalyst; sol–gel method; photodegradation; environmental remediation

1 Introduction

Global population growth and industrialization have resulted in a significant rise in environmental pollution, adversely affecting essential natural elements like air and water, which are crucial for sustaining life on Earth.[1] Water pollution, caused by the discharge of chemicals and contaminants into rivers, lakes, and oceans, affects aquatic ecosystems and poses risks to human health. Addressing these environmental challenges is essential for the well-being of both the planet and its inhabitants.[2] As a result, a wide range of toxic organic pollutants and potentially pathogenic microorganisms are being discharged into the environment, intensifying environmental concerns. It is imperative to develop high-efficiency methods for addressing these pollutants, as the severity of environmental issues continues to escalate.[3] The global challenges of environmental pollution and toxic substance production are notably evident in industrial manufacturing areas. Textile industries exacerbate these issues due to their extensive use of water in raw material preprocessing and fabric dyeing and printing, coupled with substantial consumption of synthetic chemicals and pigments.[4] This wastewater contains a diverse array of persistent coloring substances, synthetic dyes, phenols, formaldehyde, phthalates, surfactants, chlorophenols, aromatic compounds, and heavy metals, all contributing to environmental issues.[5] The textile and dyeing industry have seen an increased use of synthetic dyes due to their cost-effectiveness, excellent stability in terms of

light, temperature, and detergents, and resistance to microbial degradation, compared to natural dyes.[4,6] Methylene Blue (MB) is a widely used dye in various industries, especially for coloring silk, wool, cotton, and paper. The extensive use of MB in these industries results in significant amounts of wastewater contaminated with carcinogenic and toxic dyes, rendering the water unsafe for human consumption. The textile industry is the largest consumer of these dyes, employing highly complex compounds with diverse structural groups. This contributes substantially to water pollution.[7–9] Conventional wastewater treatment methods effectively remove many pollutants using sedimentation, filtration, adsorption, and biological processes. However, they often struggle to eliminate bio-toxic and non-degradable organic substances that persist in the water.[10] Various techniques have been developed to address the degradation of pollutants from diverse sources in wastewater. Wastewater purification methods include flocculation, coagulation, precipitation, adsorption, ion exchange, and membrane processes, with significant advancements in these areas. However, many of these approaches are often impractical for large-scale applications.[11,12] Traditional methods for treating wastewater are expensive and often insufficient in fully degrading toxic substances, resulting in less toxic byproducts. To effectively eliminate organic contaminants from water and address environmental concerns, a photocatalytic Advanced Oxidation Process (AOP) is employed.[13] Photocatalytic treatment technology is a leading advanced oxidation method for addressing environmental pollution control. It utilizes the potent oxidant hydroxyl radical (*OH) to thoroughly oxidize and break down organic pollutants into harmless inorganic compounds.[14,15] Additionally, this technology can efficiently eliminate heavy metal ions through photocatalytic reduction reactions. Photocatalysis has garnered global attention for its capacity to harness solar energy, offering a dual benefit of addressing environmental concerns and providing a renewable and sustainable energy source.[16–18] SnO_2, TiO_2, and ZnO are the most favored metal oxide semiconductors by researchers for both fundamental studies and practical applications because of their chemical stability, high reactivity, non-toxic nature, and affordability.[19,20] A high-performance photocatalyst can transform solar energy into chemical energy, facilitating various environmental and energy-related applications. These applications encompass air purification, water treatment, self-cleaning surfaces, the conversion of CO_2 into hydrocarbon fuel, and hydrogen generation from water splitting.[21,22] Titanium dioxide (TiO_2) is one of the representatives of metal oxides (semiconductors) that have been employed in various applications, because of its cost-effectiveness, nontoxicity, physical and chemical stability, and natural abundance. Some of these applications include photodetectors, hydrogen generation, degradation of pollutants, and dye-sensitized solar cells.[23–27] TiO_2 is recognized as a highly effective photocatalyst for the degradation of diverse environmental pollutants, including bacteria, viruses, and organic

substances.[28] The primary challenge with using TiO_2 as a catalyst is its low photo quantum yield, mainly caused by the rapid recombination of photo-induced electrons and holes. Additionally, pure TiO_2 is not active under visible light due to its wide band gap, particularly in its anatase form (3.18 eV).[29] There are various techniques for synthesizing TiO_2 which include sol–gel, spray pyrolysis, solvothermal, microemulsion, precipitation, and electrochemical synthesis approaches.[30] Of the available synthesis techniques, the sol–gel method is particularly convenient and well-suited for producing nanomaterials. It stands out because it doesn't necessitate complex setups, and the synthesis occurs at standard pressure and temperature conditions.[31] The sol–gel method is the preferred and widely employed approach for TiO_2 nanoparticle synthesis due to its simplicity, cost-effectiveness, and versatility. This method allows for the formation of TiO_2 nanoparticles with various morphologies, including particles, rods, sheets, wires, tubes, aerogels, and mesoporous structures.[32,33] Wet impregnation and sol-gel techniques were employed for the preparation of TiO_2 and cobalt–sulfur TiO_2 nanostructures for water purification using a photocatalytic process. The rate of dye degradation by Co–S doped TiO_2 was observed to be higher than the pristine TiO_2 nanostructure. Meanwhile, all the prepared Co–S doped TiO_2 nanocomposites exhibited enhanced photodegradation characteristics.[34] An ionic liquid-assisted hydrothermal approach was utilized to synthesize Li-dope TiO_2 nanoparticles for photocatalytic degradation of organic dye and toxicity reduction of Cr^{6+} to non-toxic Cr^{3+}. The photodegradation studies exhibited an excellent photocatalytic activity of Li-doped TiO_2 nanocomposites, as well as a detoxification agent for toxicity reduction.[35] Magnesium-doped titanium dioxide with various dopant concentrations magnesium has been synthesized via a sol–gel approach and reported for photocatalytic degradation of dyes. The Mg^{2+}–TiO_2 photocatalysts were observed to possess enhanced photodegradation activity in methyl orange dye under visible light than the undoped TiO_2. The improved degradation obtained was attributed to the dopant concentrations of the Mg^{2+}–TiO_2 photocatalyst.[36] In the same vein, Shivaraju et al., reported a polyscale Mg-doped TiO_2 using sol–gel techniques for photocatalytic application under visible light. The photocatalyst showed excellent photodegradation under natural sunlight in both textile wastewater and modeled industrial dyes.[37] Both sol–gel and hydrothermal methods were employed by Dodoo-Arhin et al., to prepare a mesoporous titanium dioxide nanostructure with a high surface area and subsequently used for the photodegradation of Rhodamine B and Sudan III dyes, under ultra-violent light. The as-synthesized nanoparticles showed promising potential in the light-aided decomposition of dye pollutants applications.[38] The effectiveness of samarium doped titanium dioxide (Sm:TiO_2) was investigated for the photocatalytic degradation of Rhodamine B dye under the exposure of sunlight. The pristine TiO_2 and Sm-doped TiO_2 nanoparticles were synthesized via photolysis techniques with different dopant

concentrations of Sm^{3+} (1, 3 and 5 wt%). The efficiency of the photodegradation activity of Rhodamine B using Sm:TiO_2 (5 wt%) nanoparticles was observed to have reached 89 % after 120 min while varying the catalyst dosage, pollutant dosage, pH, and temperature.[39] A visible light-aided photocatalytic activity for the degradation of methyl orange dye was investigated using MoO_3–Ag co-doped TiO_2 as an enhanced novel heterogeneous photocatalyst. The study suggests that MoO_3–Ag co-doped TiO_2 nanocomposite is highly promising for the removal of wastewater and can regarded as one of the important methods for the dye pollutant in wastewater treatment.[40] The highlights of the previous works are summarized in Table 1 below.

While TiO_2 has demonstrated effectiveness in various photocatalytic systems, its performance is hindered by inherent features such as low conductivity and wide band gap, which impose limitations on its photocatalytic efficiency.[41,42] Introducing metal and non-metal ions as dopants modifies the electronic structure and optical characteristics of TiO_2 particles. This alteration aims to enhance their reactivity, reduce electron–hole pair recombination rates, and improve the efficiency of interfacial charge transfer.[43] In this report, we prepared a low bandgap TiO_2 by co-doping with lithium–cobalt using the sol-gel method that can convert pollution to a harmless matter. The photodegradation efficacy of undoped and co-doped TiO_2 was studied using Methylene Blue (MB) as modeled pollutants in aqueous media. This dye is one of the significantly used dyes in various industries, and the photocatalytic degradation efficiency of the catalysts using the modeled dye shows high photodegradation efficacy. Therefore, this research work will establish the effect of TiO_2 co-doping with lithium–cobalt as an effective material for photocatalysis and

Table 1: Summary of the reported previous works.

Photocatalyst	Preparation methods	Pollutants (dyes)	Degradation (%)	Time (min)	References
Co–S doped TiO_2	Sol–gel	Brilliant green	65	75	34
Li-doped TiO_2	Ionic–liquid assisted hydrothermal	Trypan blue	75	120	35
Mg-doped TiO_2 (0.25–1.0 wt%)	Sol–gel	Methyl orange	95	250	36
Mg-doped TiO_2	Sol–gel	Industrial dyes Textile water	65–95 92	300	37
TiO_2	Sol–gel	Rhodamine B Sudan III dyes	94 100	150	38
Sm:TiO_2	Photolysis	Rhodamine B	89	120	39
MoO_3–Ag doped TiO_2	Sol–gel	Methyl orange	97	300	40

comparison of co-doping semiconductors with two types of atoms for better photocatalytic activities.

2 Experimental details

2.1 Preparation of pure TiO_2

Pure TiO_2 photocatalysts are synthesized by sol–gel method with a starting precursor of titanium isopropoxide or TTIP ($C_{12}H_{28}O_4Ti$). 13 ml of 2-propanol was dropped into a beaker and 10 ml of acetic acid was added slowly. The solution was stirred for a few minutes, after which 5 ml TTIP was added to the solution, and it was stirred vigorously with the aid of a magnetic stirrer for 15 min 61 ml of de-ionized water was added drop wisely to the solution and stirred continuously for 4 h. Consequently, the obtained solution was aged for 24 h at room temperature. As prepared TiO_2 gel was dried at 100 °C for a few hours and the obtained powder samples were ground and annealed at 500 °C for 3 h.

2.2 Preparation of lithium–cobalt co-doped TiO_2

To prepare lithium–cobalt co-doped TiO_2, lithium nitrate, and cobalt (II) acetate tetrahydrate were dissolved in 61 ml of de-ionized water at room temperature, stirred for 30 min to obtain a solution X. Solution Y was obtained by dissolving 5 ml of TTIP into 13 ml of 2-propanol and 10 ml of acetic acid, then stirred for 30 min. Then solution X was added and dropped wisely into the solution under continuous vigorous stirring. The synthesized doped TiO_2 gel was dried for a few hours at 100 °C, and the powder was subsequently pulverized and annealed at 500 °C for 3 h.

2.3 Characterizations

The photocatalysts characterization for their crystalline structure, optical properties, surface morphology, and molecular compositions and structure were characterized. The morphology and elemental composition of the photocatalysts were analyzed with high-resolution field emission scanning electron microscopy coupled with an EDX system (FE-SEM JSM-7800 F, JOEL Ltd, Letchworth, UK). X-ray powder diffraction (XRD) was done at room temperature by Rigaku X-ray diffractometer Smartlab, with Cu (Kα) radiation-based (λ = 0.154 nm). The diffraction X-ray was collected by a diffractometer using an X'Celerator detector at 40 kV and an emission

current of 30 mA. The range of 2θ was set within a range of 20°–70° with the rotation speed of 2.016°/min and 0.01° step width. Diffuse Reflectance Spectroscopy (UV–vis DRS) was studied using a Spectrophotometer USB 4000 UV–vis detector light source (HP-2000 BAL ocean optics) with the range of 200–800 nm for the optical absorption properties of the photocatalysts. Perkin Elmer FTIR spectrometer was employed to study the Fourier transform infrared spectroscopy to identify the functional groups within the photocatalysts.

2.4 Photocatalytic experiment

The photocatalytic assessment of the nanoparticles involved the degradation of a simulated Methylene Blue (MB) dye using sunlight as the light source. All experiment parameters were held constant, except for sunlight intensity. The dye solution had a neutral pH and was prepared at a concentration of 2.5 mol/L using distilled water, and the reaction took place in a 250 mL beaker positioned on a magnetic stirrer. For each 25 mL of dye solution, 15 mg of photocatalyst was added, and the mixture was stirred for 20 min to create a suspension. The suspension was then left in the dark for 30 min to reach adsorption–desorption equilibrium before being exposed to solar irradiation for 2 h. Measurements were taken at specific time intervals (0 min, 10 min, 20 min, 30 min, 40 min, 50 min). A 2 mL aliquot was extracted from the samples and subjected to centrifugation for 5 min to facilitate separation. The resulting supernatant was then analyzed using a UV–visible spectrophotometer to determine the percentage degradation, and the absorbance readings were recorded. The degradation percentages were calculated using Lambert Beer's equation:

$$\mathrm{D} = \frac{C_\mathrm{i} - C_\mathrm{f}}{C_\mathrm{i}} \times 100\ \% \tag{1}$$

where C_i denotes the initial concentration of the dyes, and C_f signifies the final concentration of the dyes. At the same time, a control experiment was conducted with the dye solution exposed to solar irradiation in the absence of a catalyst.

3 Results and discussion

3.1 SEM-EDX analysis

The morphology and elemental composition of the photocatalysts were analyzed with field emission scanning electron microscopy coupled with an EDX system (FE-SEM JSM-7800 F, JOEL Ltd, Letchworth, UK). Figure 1(a and b) depicts the surface

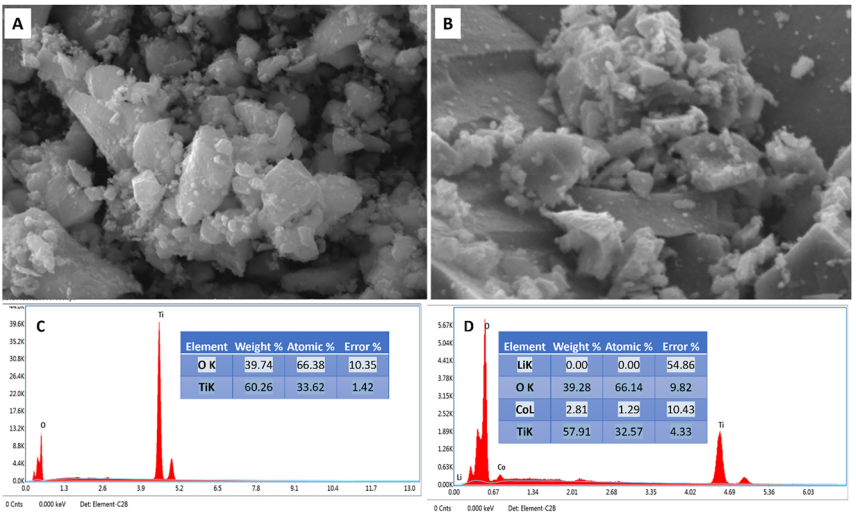


Figure 1: Morphology and elemental composition of the photocatalysts. (a and b) SEM images of TiO_2 and Li:Co-TiO_2 and (c and d) EDX spectra of TiO_2 and Li:Co-TiO_2 (inset elemental compositions [wt% and at.%] table of the photocatalysts).

morphology of the TiO_2 and Li:Co-TiO_2 photocatalysts with irregularly structured particles. The EDX elemental composition shown from the spectra in Figure 1(c and d) confirmed the inclusion of Ti, Co, Li, and O, indicating successful preparation of the TiO_2 and Li:Co-TiO_2 photocatalysts.

The inset table of elemental compositions shows the weight and atomic percentages of the photocatalysts with their respective error percentage. However, the EDX was unable to give a definite percentage composition of lithium. This is because lithium was among the light elements that EDX cannot be easily detected due to their very low energy characteristics radiation. Moreover, Li is one of the most highly reactive and oxidized elements when exposed to air.[44] The EDX mapping studies of the elemental distribution of TiO_2 and Li:Co-TiO_2 photocatalysts were recorded at high magnifications of 10 µm and 20 µm respectively, as shown in Figure 2(a–d) and Figure 3(a–f). The analysis revealed the distribution of Ti, O, with the inclusion of Co and Li, affirming the successful co-doping of the TiO_2.

3.2 XRD analysis

Figure 4 shows the X-ray diffraction pattern of TiO_2 and lithium–cobalt doped TiO_2 photocatalysts recorded from 20° to 70°. The XRD peaks for both pure and doped

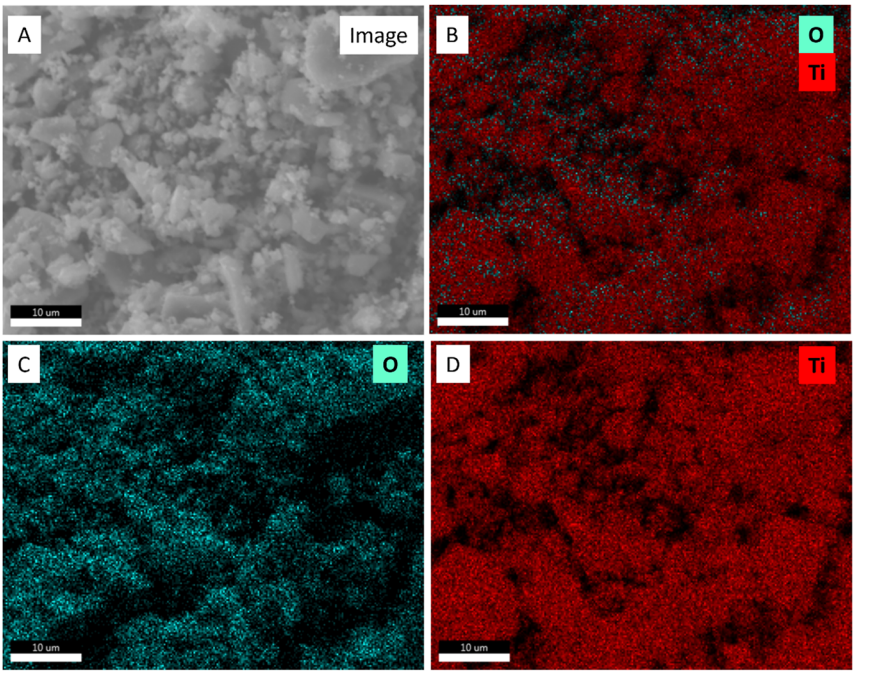


Figure 2: EDX mapping of TiO_2. (a–d) Elemental distribution and mapping of TiO_2 photocatalyst.

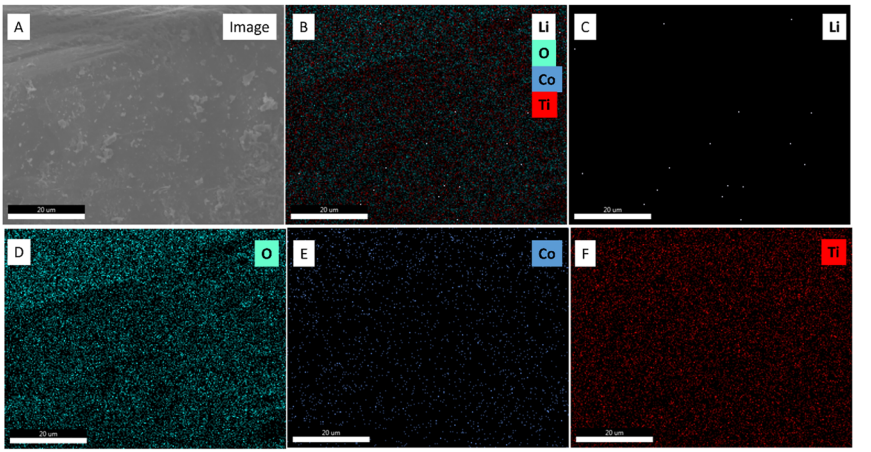


Figure 3: EDX mapping of Li:Co-TiO_2. (a–f) Elemental distribution and mapping of Li:Co-TiO_2 photocatalyst.

(TiO_2 and Li:Co-TiO_2) photocatalysts are characteristics of anatase TiO_2 structure with a tetragonal crystal phase system. The values of the 2Θ peaks 25.72°, 37.29°, 38.27°, 48.32°, 54.29°, 55.31°, 63.07°, and 69.28° correspond to the diffraction indexed planes of (101), (112), (004), (200), (105), (211), (204) and (116) respectively. The diffraction patterns corresponded with JCPDS standard card number: 01-073-1764, and the diffractograms exhibit the tetragonal anatase phase structure of TiO_2, as the characteristic structure stable after the addition of Li–Co dopants. This indicated that doping Li–Co with TiO_2 has not significantly altered the crystal structure of the materials.[34,35,45] However, there was a slight shift to a higher value in the highly intense peak of diffraction at 25.27° which can be attributed to the lithium–cobalt insertion. The average crystallite size of TiO_2 and Li:Co-TiO_2 photocatalysts were respectively found to be 14.2 nm and 13.9 nm using the Debye–Scherrer formula.

$$D = \frac{K\lambda}{\beta \cos \theta} \tag{2}$$

where D is the average crystalline size in (nm), K is the shape factor (0.9), λ is the wavelength, β is line width at maximum intensity, and Θ is the Braggs angle.

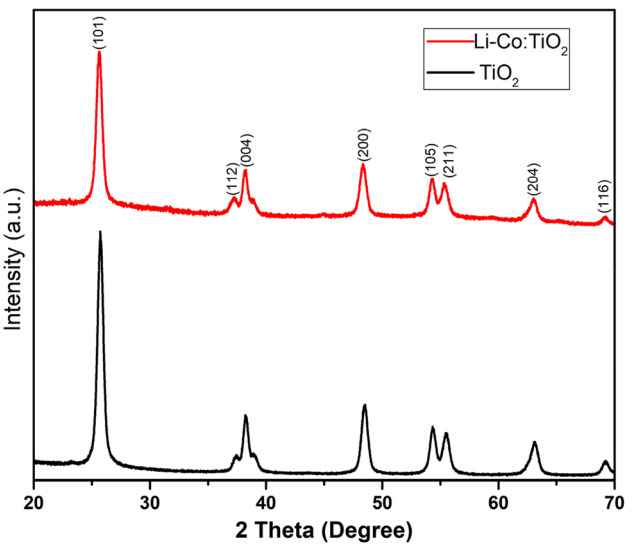


Figure 4: X-ray diffraction pattern of TiO_2 and Li:Co-TiO_2 photocatalysts.

3.3 Diffuse Reflectance Spectroscopy (DRS study)

Figure 5(a and b) illustrates the optical properties of the pure TiO_2 and Li:Co-TiO_2 determined by diffuse reflectance scattering (DRS) across the wavelength range of 200–800 nm. Figure 3(a) shows that TiO_2 has a broad absorbance band at the wavelengths of 389 nm, indicating that its range of photoactivity is restricted to the UV part of the spectrum. The Li:Co-TiO_2 band showed that there is a red shift of the absorption band toward wavelengths higher than 400 nm, with the addition of dopants. This also implied that Li:Co-TiO_2 has higher absorption spectra than TiO_2 for the visible and UV light spectrum. The reflectance spectra of both TiO_2 and co-doped TiO_2 were presented in Figure 5(b), which displayed slightly redshifted spectra towards lower wavelengths with the addition of Li and Co dopant. The reflectance that takes place in optical transitions causes a significant peak to be noticed at approximately 400 nm. The observed characteristics of the spectra were well correlated with the Ould Ne et al.[46] The DRS spectrum was used to calculate the energy bandgap using the KubelkaMunk relation, as shown in Equation (3).

$$F(R) = \frac{(1-R)^2}{2R} \tag{3}$$

where R is the reflectance, $F(R)$ is proportional to the extinction coefficient (α).

The estimated energy band gap for the corresponding wavelengths of both undoped and Li:Co doped TiO_2, was calculated to be 3.26 eV and 2.8 eV respectively. The remarkable decrease in the energy band gap of Li:Co doped TiO_2 can be attributed to the substitution of the dopants in the pristine lattice structure of TiO_2,

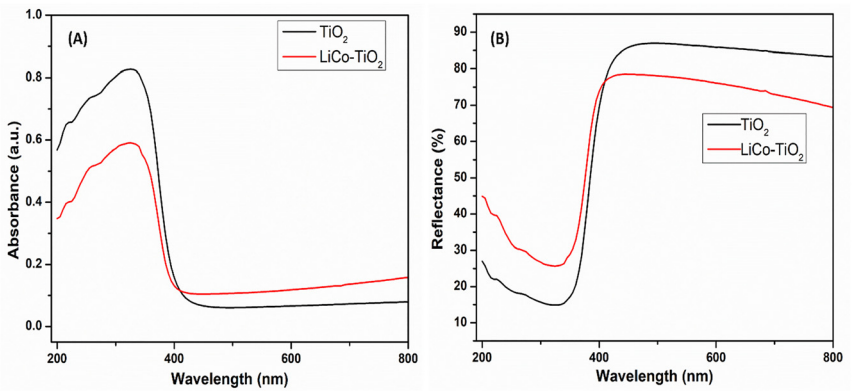


Figure 5: DRS plots of TiO_2 and Li:Co-TiO_2. (a) Absorbance and (b) reflectance spectra of TiO_2 and Li:Co-TiO_2 from DRS.

which introduced oxygen ion vacancies and additional energy states near the valence band.[47,48] Therefore, lower energy photons may be used to stimulate the valence band of the modified samples, and thereby exhibit excellent photo-degradation activity of dye under visible and UV irradiation.

3.4 Fourier transform infrared spectroscopy (FT-IR)

FT-IR spectroscopy was conducted to identify the functional groups within the prepared samples (see Figure 6). The spectra of co-doped TiO_2 exhibit a prominent absorption band in the range of 3,200–3,400 cm^{-1}, attributed to the stretching vibration mode of the hydroxyl bond (–OH). Additionally, an absorption band at around 880 cm^{-1} corresponds to the bending mode of –OH vibration associated with adsorbed water molecules in the prepared photocatalysts.[49] Low-frequency analysis revealed a notable band within the 500–880 cm^{-1} range across all samples, signifying the presence of the O=Ti=O bond, which confirms the formation of TiO_2. These vibration patterns closely resemble those observed in the pristine TiO_2 sample.[34] However, for the co-doped sample, characteristics peak around 1,600 cm^{-1} was observed, and validates the incorporation of Li:Co atom in the TiO_2 lattice. The peaks at 722 and 500 cm^{-1} arise due to the Ti=O bond stretching mode of the anatase polymorph of the TiO_2, corresponding to the M–O bonds.[50] In addition, the

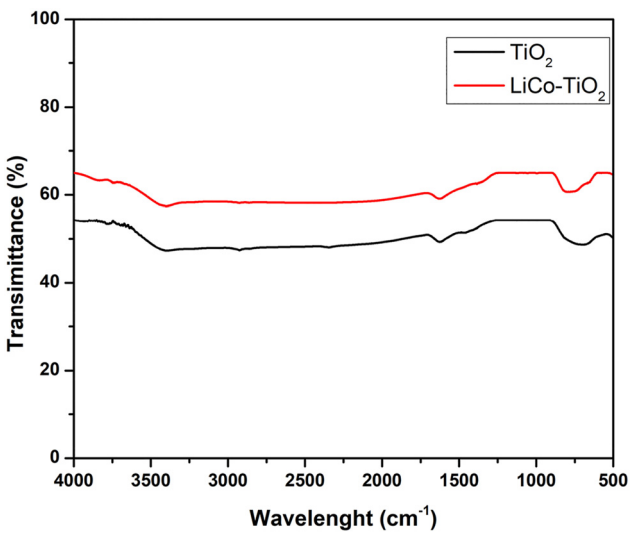


Figure 6: FT-IR spectra for TiO_2 and Li:Co-TiO_2 samples.

characteristic peaks for the Li:Co-TiO_2 were observed at 500–880, 500–800 cm^{-1}, confirming the successful preparation of TiO_2, and Li:Co doped TiO_2.

3.5 Photocatalytic activity

Photocatalytic performance was assessed for both TiO_2 and Li:Co-TiO_2 photocatalysts through the degradation of MB dye under solar light exposure. As potential photocatalysts in the reduction of MB-simulated water to a colorless aqueous solution with the aid of sunlight, TiO_2 and Li:Co-TiO_2 were employed in the photodegradation of MB dyes. All the experiments were conducted within the same period with an average solar intensity of 92,000 ± 1,000 lx.

In Figure 7(a and b), the absorption spectra depict an aqueous solution comprising 25 ml of MB and 15 mg of the photocatalysts subjected to solar light irradiation over different time intervals. The UV–vis absorbance spectrum was measured within the 200–900 nm range, and the peak absorbance for MB dyes was observed at 650 nm. It can be observed that the absorption peaks rapidly decrease with an increase in the irradiation time (50 min) with the aid of photocatalysts and sunlight, indicating the degradation of MB. The intense blue of the MB solution also faded periodically and became colorless during the degradation process. Throughout the degradation process of the MB solution, its vivid blue gradually diminished and eventually turned colorless. The percentage photodegradations of MB solution is shown in Figure 8. It implies the quantitative representation of the degraded dye, and

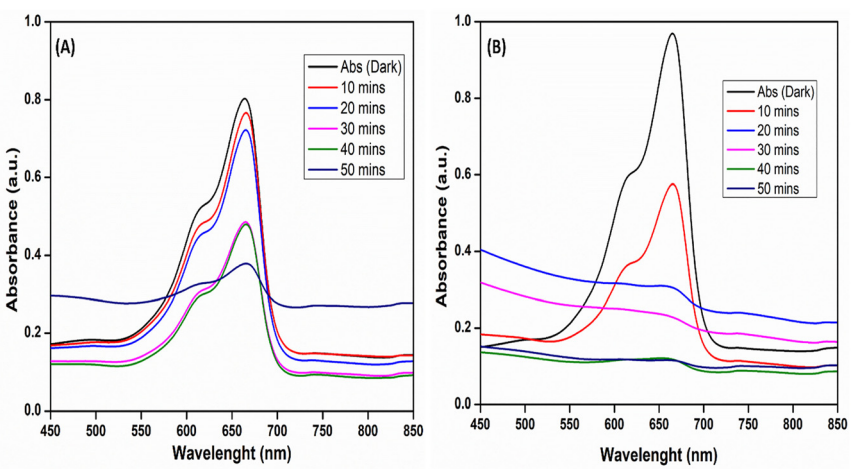


Figure 7: Absorbance spectra of MB solution under solar irradiation for (a) TiO_2 and (b) Li:Co-TiO_2.

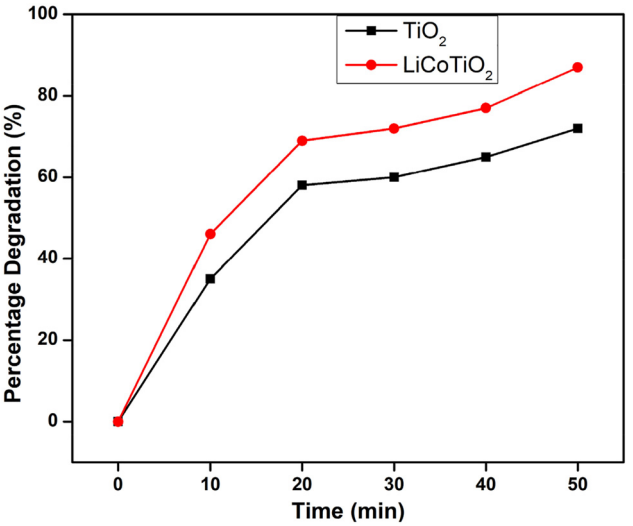


Figure 8: Photodegradation of MB dye using TiO_2 and Li:Co-TiO_2 photocatalysts.

it was shown that as the exposure time increases, the photocatalytic degradation proportionally increased, respectively. It was evident from the figure that the photodegradation of TiO_2 was considerably enhanced by the co-doping of Li:Co and degraded faster than the pure TiO_2 photocatalyst. The total amount of the degraded MB dye within the total time interval of the irradiation was recorded to be 72 % and 87 % for TiO_2 and Li:Co co-doped TiO_2 respectively. Therefore, Li:Co co-doped TiO_2 photocatalyst displayed an improved photocatalytic activity than the TiO_2 photocatalyst, as the irradiation time increased.[51] The decreased energy band gap obtained for the Li:Co co-doped TiO_2 could be accountable for their photodegradation improvement. Likewise, the oxygen defects and the increased surface area resulting

Table 2: Comparison of the degradation efficiency for Li:Co co-doped TiO_2 photocatalysts.

Photocatalyst	Preparation methods	Pollutants (dyes)	Degradation (%)	Time (min)	References
Co–S doped TiO_2	Sol–gel	Brilliant green	65	75	34
MoO_3–Ag doped TiO_2	Sol–gel	Methyl orange	97	300	40
Li:Co-doped TiO_2	Sol–gel	Methylene blue	87	50	This work

from the incorporation of Li:Co, significantly enhanced the photocatalytic performance. The comparison table for the degradation efficiency for Li:Co co-doped TiO_2 with literature was presented in Table 2.

3.6 Photodegradation mechanisms of Li:Co co-doped TiO_2 photocatalysts

Figure 9 shows the photocatalytic mechanisms of Li:Co co-doped TiO_2 photocatalyst, which was postulated on the electron–hole charge carrier photogeneration and their respective separation. The electron–hole pairs produced from the irradiated TiO_2, and the electron–hole pairs recombination reduced the rate of photodegradation. Electrons (e^-) in the valance band (VB) can be transported to the conduction band (CB) during the photocatalytic process, whereas holes (h^+) of the same quantity are created in the VB. These pairings of (e^-/h^+) generated through sunlight can facilitate chemical interactions with organic contaminants. Hydroxyl radicals (*OH) are produced during the chemical reaction between the hydroxide ions or H_2O adsorbed on the surface of the photocatalysts and the holes in the VB.[52] Electrons in the CB, on the other hand, can reduce O_2 to form superoxide radicals ($*O_2^-$) and then additional reactive oxygen species (i.e., H_2O_2 and OH^-). Due to their extreme reactivity toward organic contaminants, holes and OH as oxidation agents have positive effects on the degradation of dyes.[53] The e^-/h^+ volume recombination rate should decrease because of size reduction, permitting photogenerated e^-/h^+ pairs to travel to the surface via a short pathway and increasing photocatalytic activity.[54] The capacity of the dopants

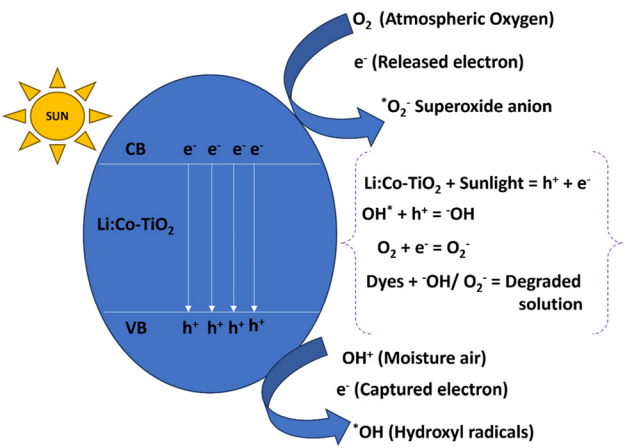


Figure 9: Graphical illustration for the possible photocatalytic mechanisms of Li:Co-TiO_2.

(lithium–cobalt) to trap electrons may have contributed to the reduction of light-generated electron–hole pair recombination at the TiO_2 surface, which in turn led to a more efficient electron transfer to donors and acceptors adsorbed on the particle surface. This would account for the positive effect of lithium–cobalt on the photocatalytic activity of TiO_2 in MB dye degradation.[35,55,56]

4 Conclusions

TiO_2 and Li:Co-TiO_2 composites were successfully prepared by a simple sol–gel method. The XRD results showed an anatase phase of TiO_2 with an average crystallite size of 14.2 nm and 13.9 nm for the photocatalysts and FTIR revealed the formation of TiO_2 and Li–Co–TiO_2 nanostructures formation. The optical results from DRS showed the reduction in the bandgap of the synthesized materials with the incorporation of Li:Co dopant to the TiO_2 composites. FESEM studies revealed the surface morphology of the photocatalysts to be irregularly structured spherical-like particles, and the EDX spectra showed the presence of Ti, Co, Li, and O, signaling successful preparation of the photocatalysts. The potential applications in photocatalytic activities of the materials showed an excellent photodegradation of MB dye. Also, the improved degradation of MB when using Li:Co-TiO_2 implied that the composite photocatalyst would be a better candidate than pristine TiO_2. The overall amount of the degraded MB dye within the complete time interval of the irradiation was found to be 72 % and 87 % for TiO_2 and Li:Co co-doped TiO_2 respectively. The improvement in the percentage degradation of MB by Li:Co-TiO_2 photocatalyst can be associated with the narrowed bandgap of the materials. Therefore, the results will proffer a better understanding and pave the way for new materials as excellent composites for photocatalysis and water treatment applications.

Research ethics: Not applicable.
Author contributions: All authors have read and agreed to the published version of the manuscript.
Competing interests: The authors declare that they have no known competing financial interests or personal relationships that could have appeared to influence the work reported in this paper.
Research funding: OA gratefully acknowledges the Department of Science & Technology (Govt. of India) for the award of the 2019/2020 Research Training Fellowship for Developing Countries Scientists (RTF-DCS). The authors extend their thanks to Researchers Supporting Project (Ref: RSPD2024R740), King Saud University, Riyadh, Saudia Arabia.
Data availability: All the data used in the manuscript are within the manuscript.

References

1. Liu, H.; Wang, C.; Wang, G. *Chem. Asian. J.* **2020**, *15*, 3239.
2. Manisalidis, I.; Stavropoulou, E.; Stavropoulos, A.; Bezirtzoglou, E. *Front Public Health* **2020**, *8*, 1.
3. Kareem, M. A.; Bello, I. T.; Shittu, H. A.; Sivaprakash, P.; Adedokun, O.; Arumugam, S. *Cleaner Mater.* **2022**, *3*, 100041.
4. Yaseen, D. A.; Scholz, M. *Textile Dye Wastewater Characteristics and Constituents of Synthetic Effluents: A Critical Review*; Springer: Berlin Heidelberg, 2019.
5. Babu, B. R.; Parande, A. K.; Raghu, S.; Kumar, T. P. *Rev. Mex. Ing. Quim.* **2023**, *22*, 141.
6. Azanaw, A.; Birlie, B.; Teshome, B.; Jemberie, M. *Case Stud. Chem. Environ. Eng.* **2022**, *6*, 100230.
7. Khan, I.; Saeed, K.; Zekker, I.; Zhang, B.; Hendi, A. H.; Ahmad, A.; Ahmad, S.; Zada, N.; Ahmad, H.; Shah, L. A.; Shah, T.; Khan, I. *Water* **2022**, *14*, 242.
8. Fong, W. M.; Affam, A. C.; Chung, W. C. *Int. J. Environ. Sci. Technol.* **2020**, *17*, 3485.
9. Pandey, S.; Do, J. Y.; Kim, J.; Kang, M. *Int. J. Biol. Macromol.* **2020**, *143*, 60.
10. Danish, M. S. S.; Estrella, L. L.; Alemaida, I. M. A.; Lisin, A.; Moiseev, N.; Ahmadi, M.; Nazari, M.; Wali, M.; Zaheb, H.; Senjyu, T. *Metals* **2021**, *11*, 1.
11. Shrestha, R.; Ban, S.; Devkota, S.; Sharma, S.; Joshi, R.; Tiwari, A. P.; Kim, H. Y.; Joshi, M. K. *J. Environ. Chem. Eng.* **2021**, *9*, 105688.
12. Ahmed, M. K.; Shalan, A. E.; Afifi, M.; El-Desoky, M. M.; Lanceros-Méndez, S. *ACS Omega* **2021**, *6*, 23129.
13. Stasinakis, A. S. *Global Nest J.* **2008**, *10*, 376.
14. Sakthivel, S.; Paramasivam, S.; Velusamy, P.; Jerries Infanta, J. A. D.; Ragavendran, V.; Mayandi, J.; Arumugam, S.; Kim, I. *Z. Phys. Chem.* **2024**, *238*, 1.
15. Karuppaiya, V.; Arangarajan, V.; Rajendran, V.; Kim, I.; Hasan, I.; Paramasivam, S. *Z. Phys. Chem.* **2024**, *238*, 1.
16. Kumari, P.; Kumar, A. *Results Surf. Interfaces* **2023**, *11*, 100122.
17. Guo, W.; Guo, T.; Zhang, Y.; Yin, L.; Dai, Y. *Chemosphere* **2023**, *339*, 139486.
18. Aarthi, A.; Umadevi, M.; Parimaladevi, R.; Sathe, G. V.; Arumugam, S.; Sivaprakash, P. *J. Inorg. Organomet. Polym. Mater.* **2021**, *31*, 1469.
19. Shittu, H. A.; Adedokun, O.; Kareem, M. A.; Bello, I. T.; Arumugam, S. *Biointerface Res. Appl. Chem.* **2023**, *13*, 1.
20. Velmurugan, G.; Ganapathi Raman, R.; Sivaprakash, P.; Viji, A.; Cho, S. H.; Kim, I. *Nanomaterials* **2023**, *13*, 1.
21. Wang, W.; Wong, P. K.; Pillai, S. C.; Ming, T.; Dunlop, P. S. M. *Int. J. Photoenergy* **2016**, *2016*, 2.
22. Si, H.; Zhou, M.; Fang, Y.; He, J.; Yang, L.; Wang, F. *Constr. Build. Mater.* **2021**, *298*, 123835.
23. Cano-Casanova, L.; Amorós-Pérez, A.; Ouzzine, M.; Lillo-Ródenas, M. A.; Román-Martínez, M. C. *Appl. Catal. B* **2018**, *220*, 645.
24. Qin, Y.; Wang, Z.; Jiang, J.; Xing, L.; Wu, K. *Chem. Eng. J.* **2020**, *394*, 124917.
25. Hernández-Ferrer, J.; Ansón-Casaos, A.; Víctor-Román, S.; Sanahuja-Parejo, O.; Martínez, M. T.; Villacampa, B.; Benito, A. M.; Maser, W. K. *Electrochim. Acta* **2019**, *298*, 279.
26. Chahrour, K. M.; Yam, F. K.; Eid, A. M. *Ceram. Int.* **2020**, *46*, 21471.
27. Jubu, P. R.; Chahrour, K. M.; Yam, F. K.; Awoji, O. M.; Yusof, Y.; Bee Choo, E. *Sol. Energy* **2022**, *235*, 152.
28. Nakano, R.; Hara, M.; Ishiguro, H.; Yao, Y.; Ochiai, T.; Nakata, K.; Murakami, T.; Kajioka, J.; Sunada, K.; Hashimoto, K.; Fujishima, A.; Kubota, Y. *Catalysts* **2013**, *3*, 310.
29. Nguyen Thi Thu, T.; Nguyen Thi, N.; Tran Quang, V.; Nguyen Hong, K.; Nguyen Minh, T.; Le Thi Hoai, N. *J. Exp. Nanosci.* **2016**, *11*, 226.

30. Suhan, M. B. K.; Al-Mamun, M. R.; Farzana, N.; Aishee, S. M.; Islam, M. S.; Marwani, H. M.; Hasan, M. M.; Asiri, A. M.; Rahman, M. M.; Islam, A.; Awual, M. R. *Nano-Struct. Nano-Objects* **2023**, *36*, 101050.
31. Paramasivam, G.; Palem, V. V.; Sundaram, T.; Sundaram, V.; Kishore, S. C.; Bellucci, S. *Nanomaterials* **2021**, *11*, 1.
32. Bokov, D.; Turki Jalil, A.; Chupradit, S.; Suksatan, W.; Javed Ansari, M.; Shewael, I. H.; Valiev, G. H.; Kianfar, E. *Adv. Mater. Sci. Eng.* **2021**, *2021*, 1.
33. Akpan, U. G.; Hameed, B. H. *Appl. Catal. A Gen.* **2010**, *375*, 1.
34. Hafeez, M.; Afyaz, S.; Khalid, A.; Ahmad, P.; Khandaker, M. U.; Sahibzada, M. U. K.; Ahmad, I.; Khan, J.; Alhumaydhi, F. A.; Bin Emran, T.; Idris, A. M. *J. King Saud Univ. Sci.* **2022**, *34*, 102028.
35. Ravishankar, T. N.; Nagaraju, G.; Dupont, J. *Mater. Res. Bull.* **2016**, *78*, 103.
36. Kiran Avasarala, B.; Tirukkovalluri, S. R. *J. Environ. Anal. Toxicol.* **2016**, *6*, 1.
37. Shivaraju, H. P.; Anil, G. M. K. M.; Pallavi, K. S.; Pallavi, N.; Behzad, S. *Appl. Water. Sci.* **2017**, *7*, 3937.
38. Dodoo-Arhin, D.; Buabeng, F. P.; Mwabora, J. M.; Amaniampong, P. N.; Agbe, H.; Nyankson, E.; Obada, D. O.; Asiedu, N. Y. *Heliyon* **2018**, *4*, 1.
39. Mahmoud, Z. H.; AL-Bayati, R. A.; Khadom, A. A. *J. Mol. Struct.* **2022**, *1253*, 132267.
40. Hasan Khan Neon, M.; Islam, M. S. *Environ. Nanotechnol. Monit. Manag.* **2019**, *12*, 100244.
41. Kang, X.; Liu, S.; Dai, Z.; He, Y.; Song, X.; Tan, Z. Titanium Dioxide: From Engineering to Applications. *Catalysts* **2019**, *9*, 1,
42. Nasr, M.; Eid, C.; Habchi, R.; Miele, P.; Bechelany, M. *Chem. Sus. Chem.* **2018**, *11*, 3023.
43. Etacheri, V.; Di Valentin, C.; Schneider, J.; Bahnemann, D.; Pillai, S. C. *J. Photochem. Photobiol. C Photochem. Rev.* **2015**, *25*, 1.
44. Muto, S.; Tatsumi, K. *Microscopy* **2017**, *66*, 39.
45. Nguyen, T. M. H.; Bark, C. W. *ACS Omega* **2020**, *5*, 2280.
46. Ould Ne, M. L.; Abbassi, A.; El hachimi, A. G.; Benyoussef, A.; Ez-Zahraouy, H.; El Kenz, A. *Opt. Quantum Electron.* **2017**, *49*, 1.
47. Khurana, C.; Pandey, O. P.; Chudasama, B. *J. Solgel Sci. Technol.* **2015**, *75*, 424.
48. Serpone, N.; Lawless, D.; Khairutdinov, R. *J. Phys. Chem.* **1995**, *99*, 16646.
49. Rattan, S.; Suresh, K.; Mamta, S.; Tripathi, S. K.; Goswamy, J. *Results Mater.* **2020**, *9*, 100127.
50. Senthil Kumar, P.; Selvakumar, M.; Babu, S. G.; Jaganathan, S. K.; Karuthapandian, S.; Chattopadhyay, S. *RSC Adv.* **2015**, *5*, 57493.
51. Sharma, R.; Saini, H.; Paul, D. R.; Chaudhary, S.; Nehra, S. P. *Environ. Sci. Pollut. Res.* **2021**, *28*, 7116.
52. Sinha, T.; Ahmaruzzaman, Md; Adhikari, P. P.; Bora, R. *ACS Sustain. Chem. Eng.* **2017**, *5* (6), 4645.
53. Manjula, N.; Selvan, G.; Balu, A. R. *J. Mater. Sci. Mater. Electron.* **2018**, *29*, 3657.
54. Sarkar, S.; Ponce, N. T.; Banerjee, A.; Bandopadhyay, R.; Rajendran, S.; Lichtfouse, E. *Environ. Chem. Lett.* **2020**, *18*, 1569.
55. Dahl, M.; Liu, Y.; Yin, Y. *Chem. Rev.* **2014**, *114*, 9853.
56. An, X.; Yu, J. C. *RSC Adv.* **2011**, *1*, 1426.